Applied Catalysis B: Environmental 303 (2022) 120884

Contents lists available at ScienceDirect

Applied Catalysis B: Environmental

journal homepage: www.elsevier.com/locate/apcatb

Peroxide activation by microbially synthesized sulfidated iron: Comparison against abiotic iron-based materials in terms of treatment efficiency and oxidative degradation pathway

Bowen Yang [a], Sae-In Suh [a], Jeonggil Lee [b], Hwa-Soo Ryoo [a], So-Young Ham [a], Jaesung Kim [a], Young-Jin Ko [c], Heesoo Woo [d], Jaemin Choi [a], Hyung-Suk Oh [c,e], Sang-Hoon Lee [a], Hee-Deung Park [a], Man Jae Kwon [b], Hongshin Lee [a,*], Jaesang Lee [a,*]

[a] Civil, Environmental, and Architectural Engineering, Korea University, Seoul 02841, South Korea
[b] Earth and Environmental Sciences, Korea University, Seoul 02841, South Korea
[c] Clean Energy Research Center, Korea Institute of Science and Technology, Seoul 02792, South Korea
[d] Water Cycle Research Center, Korea Institute of Science and Technology, Seoul 02792, South Korea
[e] KHU-KIST Conversing Science and Technology, Kyung Hee University, Seoul 02447, South Korea

ARTICLE INFO

Keywords:
Biogenic sulfidated iron
Sulfate-reducing bacteria
Peroxide activation
Sulfate radical
High-valent iron

ABSTRACT

This study demonstrated the application of biogenic sulfidated iron (B-FeS), produced via anaerobic digestion of *Desulfovibrio desulfuricans* using sulfate as the terminal electron acceptor, for peroxide activation. B-FeS was assessed against chemically prepared zerovalent and sulfidated iron (ferrous sulfide and pyrite) with respect to their ability to activate peroxydisulfate (PDS) and H_2O_2. Regardless of the peroxide type, B-FeS outperformed benchmark iron activators in treating 4-chlorophenol due to its resistance to iron corrosion and the high content of reduced sulfur. The roles of oxidizing radicals were confirmed based on the effects of alcohol-based quenchers, multi-activity assessment, electron paramagnetic resonance spectral features, and product analysis. The pH-dependent efficiency of sulfoxide-to-sulfone conversion suggested that high-valent iron species acted as the secondary oxidant in all iron/peroxide systems, and the contribution was more pronounced when PDS and B-FeS were used. Microbial sulfidation as a catalyst regeneration strategy recovered the peroxide activation capacity of oxidized B-FeS.

1. Introduction

Because of their natural abundance and non-toxic nature, iron and its derivatives have been broadly recognized as homogeneous and heterogeneous environmental catalysts that initiate redox reactions for the treatment of organic and inorganic contaminants [1,2]. For instance, the electron-donating potentials of iron species caused the reductive transformation of chlorinated compounds [3] and enabled the production of reactive oxygen species via successive reduction of dissolved O_2 [4]. Iron-based materials also perform the heterolytic dissociation of peroxide bonds in simple inorganic peroxides such as hydrogen peroxide (H_2O_2), peroxymonosulfate (PMS), and peroxydisulfate (PDS) [5,6]. The key mechanism underlying peroxide activation results in the generation of highly reactive intermediates, such as hydroxyl ($^{\bullet}OH$) and sulfate radicals ($SO_4^{\bullet-}$). In contrast to the single-electron reduction of peroxides that accompanies radical formation, H_2O_2 and PDS as two-electron oxidants convert iron species into high-valent metal intermediates (e.g., Fe(IV)=O) with substrate-specific reactivity, fulfilling non-radical organic oxidation via secondary degradative pathways [7,8].

Due to biocompatibility, cost-effectiveness, and facile mass production, (nanoscale) zerovalent iron ((n)ZVI) has been successfully applied for soil and groundwater remediation based on chemical reduction and/or adsorption [9]. Among the manifold strategies to improve the treatment performance of ZVI, including surface cocatalyst deposition [10], incorporation into polymers/surfactants [11,12], and immobilization on carbon supports [13], the sulfidation of ZVI has recently been highlighted as a viable technical option [14,15]. This treatment enhances the reductive detoxification of chlorinated organic/heavy metals, while minimizing electron consumption for unproductive H_2 generation from water ($2H_2O + 2e^- \rightarrow H_2 + 2OH^-$). The increased selectivity toward the

* Corresponding authors.
E-mail addresses: ghdtlsl@korea.ac.kr (H. Lee), lee39@korea.ac.kr (J. Lee).

https://doi.org/10.1016/j.apcatb.2021.120884
Received 8 July 2021; Received in revised form 18 October 2021; Accepted 30 October 2021
Available online 5 November 2021

reductive degradation of contaminants inhibited anoxic iron corrosion, allowing sulfidated ZVI to maintain its reactivity during prolonged application [16]. In particular, electron transfer from the Fe(0) core to surface-bound Fe(II)/Fe(III) in the core-shell structure of iron sulfide was promoted via the conductive iron sulfide shell, preventing nZVI passivation and dissolution [17]. These technical benefits observed in the anoxic processes imply the potential of sulfidated (n)ZVI as an iron-based heterogeneous activator of oxygen [18] and peroxides in oxidation-based water treatment [19,20]. The high electron utilization efficiency of sulfidated nZVI enabled the preferential reduction of O_2 to $^{\bullet}OH$ via H_2O_2 as an intermediate while hindering the four-electron transfer pathway for O_2 reduction (i.e., $O_2 + 4H^+ + 4e^- \rightarrow 2H_2O$) [21]. Together with the role of S(-II) as an electron donor [22], this also promotes the Fe(II)/Fe(III) cycling (i.e., Fe(II) regeneration), enabling catalytic performance in H_2O_2 and PDS activation. Furthermore, sulfur species (e.g., SO_3^{2-}) resulting from the oxidative dissolution of pyrite (FeS_2) directly activated PMS [23]. The high resistance to corrosion makes the peroxide activation capacity of sulfidated nZVI relatively insensitive to pH variation as compared to bare nZVI [24].

Sulfidated iron materials are fabricated through (i) reductive adsorption of soluble sulfur species on solid iron materials, (ii) concomitant reduction of dissolved sulfur and iron species by chemical reductants, (iii) heat treatment of solid iron materials under a sulfur dioxide atmosphere, and (iv) mechanochemical milling of elemental iron and sulfur mixtures [14]. In particular, microbial synthesis utilizing the capability of sulfur-/sulfate-reducing bacteria (SRB) to concurrently reduce SO_4^{2-} and Fe(III) [25] is considered a feasible alternative to abiotic approaches based on the following technical merits: (i) no need for hazardous sulfur sources (e.g., Na_2S and $Na_2S_2O_3$), (ii) low energy demand, and (iii) ease of mass production. However, few studies have assessed the potential application of biosynthesized sulfidated iron for peroxide activation, whereas abiotic counterparts have often been tested as proxies to (n)ZVI. Furthermore, it is likely that biogenic sulfidated iron could differ from chemically fabricated ones in terms of peroxide activation performance and mechanisms, considering that (i) SRB are involved in the biologically mediated formation of diverse iron sulfides such as pyrite, greigite (Fe_3S_4), mackinawite (FeS_{1-x}; $0 < x < 0.07$), and pyrrhotite ($Fe_{1-x}S$; $0 < x < 0.125$) [26,27] and (ii) the reactivity of sulfidated iron is sensitive to the Fe/S ratio and their oxidation states [28].

To address the knowledge gap regarding the peroxide activation capability of biogenic iron sulfide and the degradative reaction pathways, in this study we assessed the relative position of biogenic sulfidated iron (B-FeS; prepared from the Fe(II)/SO_4^{2-} mixture using *Desulfovibrio desulfuricans*) versus abiotically prepared iron-based materials, namely ferrous sulfide (M-FeS), pyrite (B-FeS), and nZVI in terms of their capability for H_2O_2 and PDS activation. The efficiencies of the iron-based activator/peroxide systems for organic oxidation were monitored under varying peroxide dosages, catalyst loadings, and pH conditions. The primary oxidants and the their dependence on the pH and types of activator and peroxide were identified based on the (i) effects of alcohol-based scavengers, (ii) efficiencies for the conversion of methanol (MeOH), benzoic acid (BA), and methyl phenyl sulfoxide (PMSO) into formaldehyde (HCHO), 4-hydroxybenzoic acid (4-HBA), and methyl phenyl sulfone ($PMSO_2$), respectively, (iii) reactivity toward multiple organic substrates, and (iv) electron paramagnetic resonance (EPR) spectral features. Finally, repeated application of B-FeS for peroxide activation and the possibility of biological regeneration were explored based on the extent of performance reduction with increasing catalytic cycle and recovery after exposure to anaerobic microbial transformation.

2. Materials and methods

2.1. Reagents

All chemicals were of reagent or analytical grade (see Text S1 in Supplementary Information) and used without further purification. Ultrapure deionized water (> 18 MΩ cm), produced by a Milli-Q Water Purification System (Millipore), was used to prepare all experimental solutions and suspensions.

2.2. Preparation of B-FeS and nZVI

Desulfovibrio desulfuricans KCCM 41817 was purchased from the Korean Culture Center of Microorganisms (KCCM) and grown anaerobically in ATCC 1249 medium (modified Baar's medium). The medium consisted of three components: Component I – 2.0 g of $MgSO_4$, 5.0 g of sodium citrate, 1.0 g of $CaSO_4$, and 1.0 g of NH_4Cl per 400.0 mL of DI water; Components II – 0.5 g of K_2HPO_4 per 200.0 mL of DI water; Component III – 1.0 g of yeast extract, and 1.64 g of sodium acetate per 400.0 mL of DI water [29]. To determine the optimal microbial growth condition for the mass production of B-FeS, the yields of B-FeS were measured by varying the culture parameters including pH, N_2: H_2 ratio, Fe^{2+}: SO_4^{2-} ratio, acetate concentration, and temperature (Table S1 and Figs. S1–S5). The medium was prepared by mixing all the components after the pH of each component was initially adjusted to 7.5 using concentrated NaOH. One hundred milliliters of medium in 160 mL serum bottle was purged with a gaseous mixture of N_2 and H_2 in a volume ratio of 8: 2 for 30 min. The purged bottle was sealed with a butyl rubber stopper and an aluminum cap under an anaerobic headspace. The medium was sterilized by autoclaving at 121 ℃ for 15 min. After cooling down the medium at room temperature, 1 mL of 0.22 μm filter-sterilized 5% ferrous ammonium sulfate solution was added to 100 mL medium (The final concentrations of acetate, Fe^{2+}, and SO_4^{2-} in the medium were 1200 mg/L, 35.6 mg/L, and 145.5 mg/L, respectively). Then, 1% of the pre-cultured bacteria were inoculated into the medium. All inoculated serum bottles were incubated in the dark at 30 °C with shaking for 3–5 days. Microbially produced FeS was harvested by passing 100 mL of each culture through a 0.45 μm PTFE membrane (Millipore). The resultant particles were washed several times with ethanol and acetone, and preserved under an inert N_2 atmosphere. The nZVI was prepared via the chemical reduction of ferrous sulfate by sodium borohydride according to the procedure reported in our previous work [30].

2.3. Experimental procedures and analytical methods

Homogeneous and heterogeneous peroxide activation was conducted in a magnetically stirred 100 mL wide-mouth glass bottle at room temperature under air-equilibrated conditions. The experimental suspensions typically consisted of a 0.1 g/L iron-based activator, 1 mM peroxide, and 0.1 mM target substrate. The initial pH was adjusted to 3 using concentrated $HClO_4$ and NaOH in most cases and the pH marginally changed over the course of peroxide activation even though the suspensions were not buffered. To investigate the effect of pH, 2-(*N*-morpholino) ethanesulfonic acid and piperazine-*N*,*N*'-bis(ethanesulfonic acid) were used as pH 5 and 7 buffers, respectively, considering that both reagents barely serve as iron-binding ligands [7]. Aliquots of 1 mL were taken from the reactor at predetermined time intervals using a 1 mL syringe, filtered through a 0.45 μm PTFE membrane (Millipore), and transferred into a 2 mL amber glass vial containing 20 μL MeOH to scavenge any residual radical-based oxidants. The concentrations of organic compounds were monitored using high-performance liquid chromatography (HPLC, Agilent Technologies 1260) equipped with a C-18 column and a UV/Vis detector. The operating conditions, such as eluent composition and flow rate, were tuned for the optimal chromatographic quantification of each compound (details are provided in

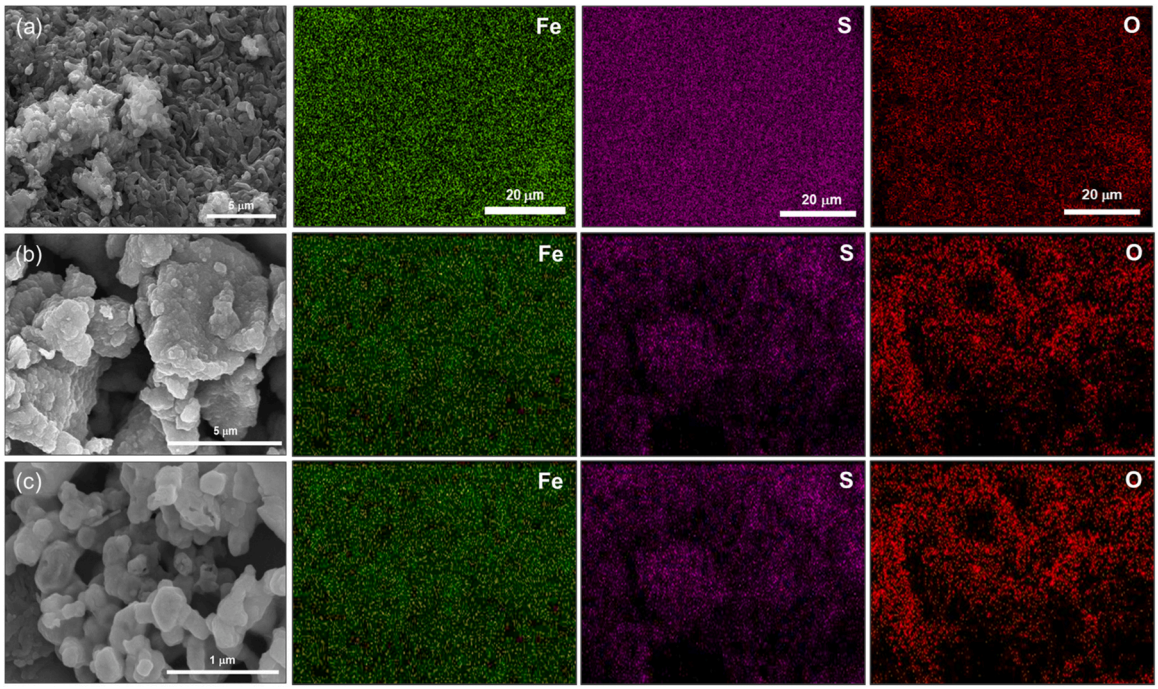

Fig. 1. SEM images of (a) B-FeS, (b) M-FeS, (c) D-FeS, and their EDS maps of element distributions.

Table S2). The intermediates generated from 4-chlorophenol (4-CP) oxidation were identified by a Q Exactive Hybrid Quadrupole-Orbitrap mass spectrometry (Thermo Fisher Scientific Inc.) in the negative electrospray ionization mode. The separation was performed on a Hypersil GOLD™aQ column using a binary mixture of 0.1% (v/v) aqueous formic acid solution and acetonitrile as the mobile phase. The intermediate analysis was also carried out by gas chromatography mass spectrometry (GC-MS, Agilent 6890/5973 GC/MSD system) equipped with a DB-5MS column (30 m × 0.25 mm, 0.25 μm). The HCHO concentration was measured by HPLC analysis (UV absorbance detection at 350 nm) after derivatization with 2,4-dinitrophenylhydrazine [31]. The initial and remaining PDS concentrations were determined according to the method suggested by Liang et al., based on the spectrophotometric quantification of iodine (λ_{max} = 352 nm) that resulted from iodide oxidation by PDS [32]. Colorimetric methods using 1,10-phenanthroline [33] and titanium sulfate [34] were used to measure the concentrations of Fe^{2+} and H_2O_2, respectively. To explore the involvement of radical-based oxidants in peroxide activation, EPR spectra were recorded on a JEOL JES-TE 300 spectrometer in 5-*tert*-butoxycarbonyl-5-methyl-1-pyrroline-*N*-oxide (BMPO) as a spin-trapping agent under the following conditions: microwave power = 0.998 mW, microwave frequency = 9.417 GHz, center field = 335.5 mT, modulation width = 0.2 mT, and modulation frequency = 100 kHz.

The surface morphology and chemical composition of the iron-based activators were analyzed using a field emission scanning electron microscope (FE-SEM, Quanta 250 FEG) equipped with an energy dispersive X-ray spectroscope (EDS, Quanta 250 FEG) and high-resolution transmission electron microscopy (HR-TEM, Talos F200X). The mineral phases of microbially and abiotically prepared iron sulfides were identified based on X-ray diffraction (XRD) patterns collected with an X-ray diffractometer (Rigaku SmartLab) using Cu-Kα radiation. The oxidation states of iron and sulfur in the iron sulfide samples were determined, and their changes were tracked by X-ray photoelectron microscopy (XPS, ULVAC-PHI X-tool) using a monochromatic Al Kα X-ray source (1486.7 eV). The Brunauer-Emmett-Teller (BET) surface areas of the iron sulfide samples were computed based on N_2 adsorption-desorption isotherms measured at − 195.8 ℃ using a gas sorption analyzer (Quantachrome Instruments, Autosorb-iQ 2ST/MP).

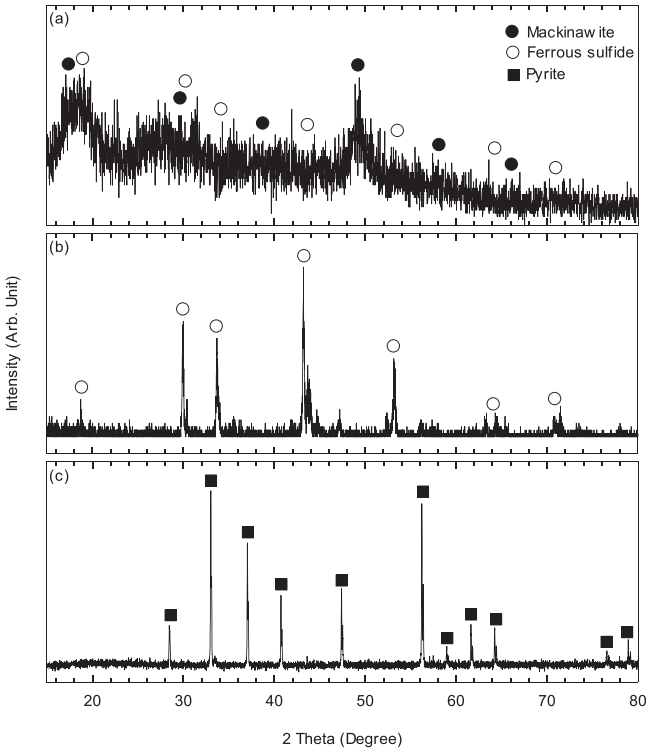

Fig. 2. XRD patterns of (a) B-FeS, (b) M-FeS, and (c) D-FeS ('arbitrary' was abbreviated to 'Arb').

3. Results and discussion

3.1. Characterization of biogenic sulfidated iron

The SEM images of sulfidated iron materials in Fig. 1 show that microbially prepared B-FeS precipitates were encrusted on curved rod-shaped *Desulfovibrio desulfuricans*, and two abiotic iron sulfides (i.e.,

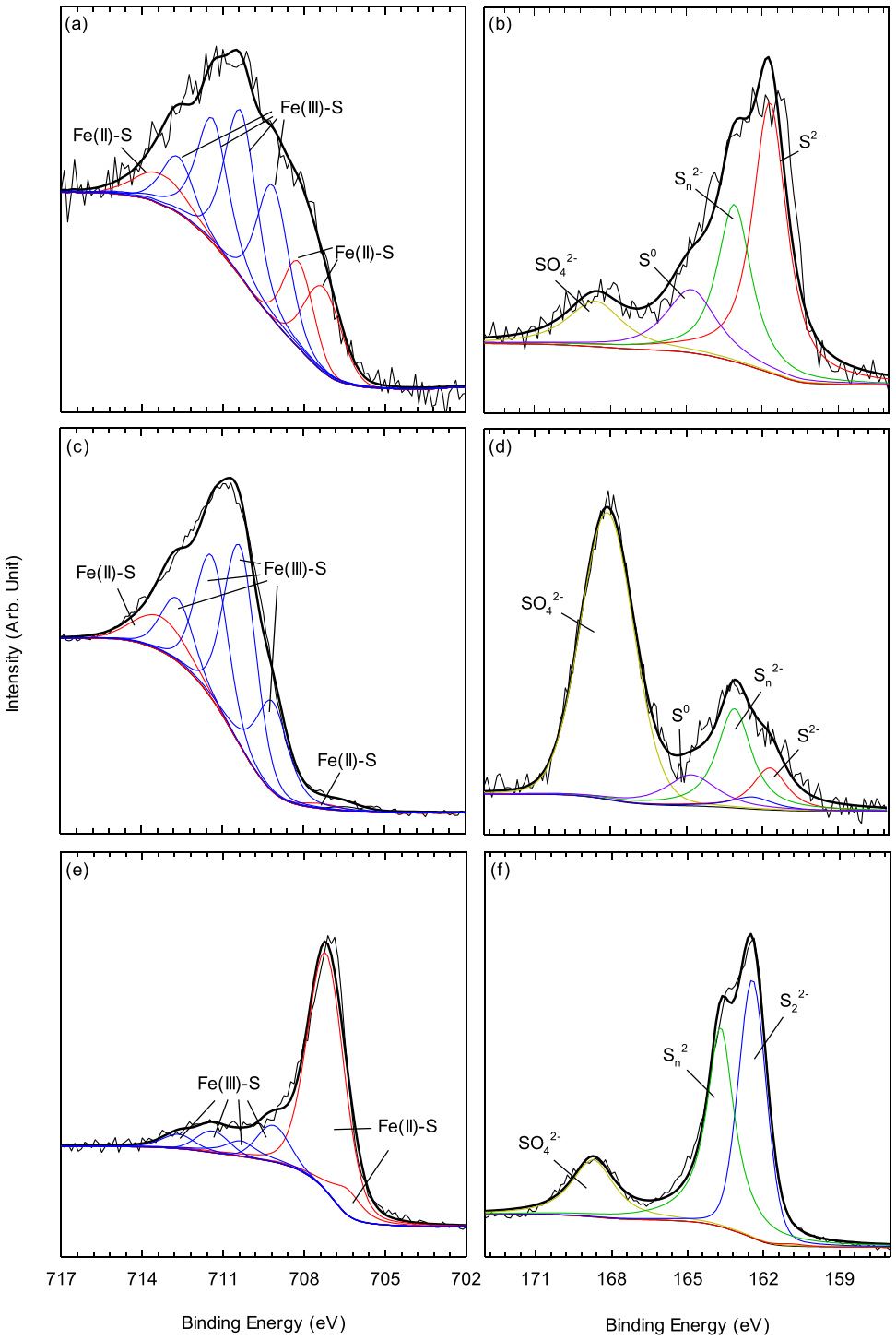

Fig. 3. Fe2p$_{3/2}$ and S2p XPS spectra of (a), (b) B-FeS, (c), (d) M-FeS, and (e), (f) D-FeS.

M-FeS and D-FeS) as non-spherical particles were highly aggregated. The M-FeS clusters were irregularly shaped and coarse-grained, but the relatively fine granularity was observed in the D-FeS sample. Agglomerates of uniform spherical particles with diameters of approximately 40–150 nm were commonly observed in the SEM images of nZVI (Fig. S6). The locally magnified TEM images further confirmed the morphological features of B-FeS (Fig. S7); individual B-FeS particles with a size of approximately 30–50 nm or their clusters were attached to the bacteria. Elemental mapping via SEM/EDS analysis indicated that iron was evenly distributed over all tested iron-based materials, and sulfur as the major component was successfully incorporated over the course of the chemical and microbial preparation of sulfidated iron (Fig. 1 and S6). The ubiquitous presence of oxygen, confirmed in the surface chemical composition analysis, would result from either iron oxides or sulfur oxyanions such as sulfite and sulfate formed on the surface of iron sulfides.

The occurrence of sharp diffraction peaks in the XRD diffractograms suggests that M-FeS and D-FeS possess a relatively high degree of crystallinity, in contrast to the broad diffraction profile of B-FeS (Fig. 2). The diffraction peaks at 29.8°, 33.7°, 43.2° and 53.2° which were indexed to the (110), (112), (114), and (300) planes, respectively, indicate that M-FeS consists of ferrous sulfide as the dominant crystalline phase (JCPDS

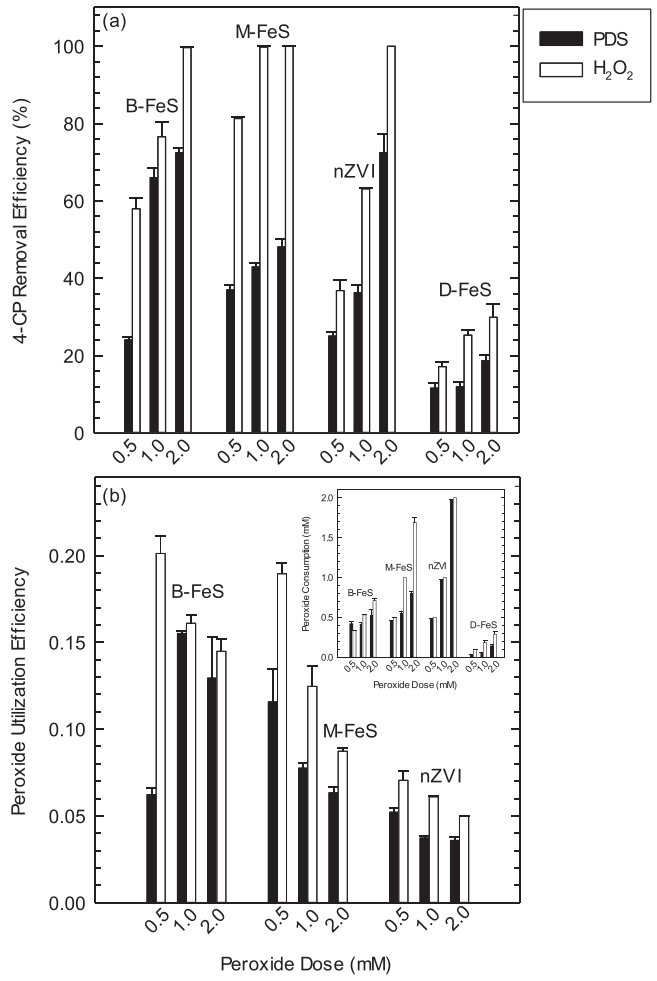

Fig. 4. Comparison of B-FeS against benchmark iron-based activators such as M-FeS, D-FeS, and nZVI in terms of efficiencies of (a) 4-CP degradation and (b) peroxide utilization in the presence of PDS and H_2O_2 at varying dosages ([iron activator]$_0$ = 0.1 g/L; [4-CP]$_0$ = 0.1 mM; pH$_i$ = 5). Inset shows peroxide consumption by all tested iron-based activators.

No. 76-0960) [35]. D-FeS was confirmed to exhibit the diffraction patterns characteristic of a pyrite crystal structure with peaks at 28.5°, 33.0°, 37.1°, 40.8°, 47.4°, and 56.3° assigned to the (111), (200), (210), (211), (220), and (311) planes, respectively (JCPDS No. 06-0710) [36]. On the other hand, B-FeS displayed diffraction patterns corresponding to a crystalline mixture containing mackinawite (JCPDS No. 15-0037) [37]. The nZVI primarily comprised body-centered cubic α-Fe^0 with a low crystalline nature based on a broad peak at 44.9°, which corresponds to the (110) plane (Fig. S8a) [38].

The presence of the mackinawite phase as a sulfur-deficient iron sulfide in B-FeS was supported by the S2p XPS spectrum, indicating that B-FeS contained sulfide (S^{2-}; S(-II)) as the main sulfur species (Fig. 3b). The S2p XPS spectra of abiotic iron sulfides showed that D-FeS consisting of pyrite possessed oxidized sulfur species, namely S_2^{2-}, S_n^{2-}, and SO_4^{2-}, and sulfur in the M-FeS had intermediate oxidation states that resulted from the co-presence of S^0, S_n^{2-}, and S^{2-} (Fig. 3d and f). SO_4^{2-} occurred in all sulfidated iron to varying degrees, which aligns well with the oxygen detection in the EDS elemental maps (Fig. 1). Spectral deconvolution performed using the multiplet peaks assigned to Fe(II)-S and Fe(III)-S implies that all sulfidated iron has a mixed iron oxidation state; Fe(III)-S existed as the predominant iron species in B-FeS and M-FeS, whereas much more intense characteristic peaks corresponding to Fe(II)-S were observed for D-FeS (Fig. 3a, c, and e). The specific peaks at ~706.1 and ~719.2 eV in the XPS spectrum of nZVI [39] confirmed the successful formation of elemental iron via chemical Fe(II) reduction though the nZVI surface was partially oxidized (Fig. S8b).

3.2. Peroxide activation capability of biogenic sulfidated iron

B-FeS was comparatively assessed against abiotic sulfidated iron (i.e., M-FeS and D-FeS) and nZVI with respect to 4-CP degradation efficiency that was monitored in the presence of peroxides, namely H_2O_2 and PDS, at varying dosages (Fig. 4a). Marginal 4-CP degradation occurred with either peroxide or iron-based activators alone, ruling out the possibility that the apparent reduction in 4-CP concentration resulted from sorption or direct oxidation by peroxides (*data not shown*). The distributions of intermediates formed during 4-CP degradation by B-FeS in the presence of PDS and H_2O_2 were distinguishable, indicating the progress of ring-opening reactions involving two different peroxide-derived radicals, that is, $SO_4^{\bullet-}$ and $^{\bullet}OH$ (Tables S3, S4, and S5; the reaction pathways for 4-CP degradation were proposed in Scheme S1). Notably, the occurrence of hydroquinone and 1,2,4,5-benzenetetrol that was linked with $^{\bullet}OH$-induced hydroxylation was unique to B-FeS/H_2O_2 whereas biphenyl derivatives formed exclusively in the B-FeS/PDS system (Table S3) (note that phenoxyl radicals primarily produced through one-electron oxidation of aromatic compounds by $SO_4^{\bullet-}$ underwent coupling reactions, transforming into dimers and trimers [40]). Regardless of the type of peroxide and activator used, the efficiency of 4-CP degradation increased in proportion to the initial peroxide dosage. B-FeS outperformed the benchmark iron-based materials in PDS activation; the performance followed the decreasing order of B-FeS > nZVI > M-FeS >> D-FeS over the PDS dosage range of 0.5–2 mM in most cases. When H_2O_2 was used instead, the position of B-FeS relative to the other heterogeneous activators changed: M-FeS > B-FeS > nZVI >> D-FeS. The comparisons collectively imply that the microbially prepared iron sulfide achieved a higher capability for peroxide activation, albeit with a slightly lower efficiency for H_2O_2 activation than that of M-FeS. Furthermore, the superiority of B-FeS as a peroxide activator was more prominent when peroxide consumption as well as 4-CP degradation efficiency was considered. For both PDS and H_2O_2, B-FeS was found to be the most effective activator based on the highest peroxide utilization efficiency, that is, the ratio of the amount of 4-CP degraded to the amount of peroxide consumed (Fig. 4b). The nZVI continued to consume peroxides in an unproductive manner (decaying peroxides without oxidant production), achieving almost complete depletion of peroxides within 1 h (Figs. S9 and S10). As a result, B-FeS exhibited two- or three-fold higher peroxide utilization efficiency than nZVI under varying peroxide dosage conditions. These results somewhat align with BET surface area since it increased in the following order: D-FeS (0.62 m^2/g) << M-FeS (10.89 m^2/g) < B-FeS (36.78 m^2/g) < nZVI (52.23 m^2/g). Aligned with the successful treatment of recalcitrant emerging contaminants by diverse peroxide activation processes that involved the formation of $SO_4^{\bullet-}$ and $^{\bullet}OH$ [2,19,22,37], B-FeS/PDS and B-FeS/H_2O_2 were confirmed to effectively decompose select pharmaceutical compounds, namely acetaminophen, carbamazepine, caffeine, and sulfamethoxazole, irrespective of their chemical structures (Fig. S11).

The possibility that *Desulfovibrio desulfuricans* (confirmed in TEM images (Fig. S7)) to remain after biogenic production of sulfidated iron caused the microbial degradation of 4-CP was explored based on the comparison of the FT-IR and Raman spectra of B-FeS and M-FeS before and after exposure to 4-CP for 1 h (Figs. S12 and S13). New characteristic peaks resulting from 4-CP adsorption on sulfidated irons (e.g., bands at 3065 cm^{-1} and 3080 cm^{-1} corresponding to aromatic C-H stretching vibration and at 1053 cm^{-1} assignable to a C-Cl moiety [41,42]) were not detected. However, the peaks indicating aliphatic hydrocarbons and oxygen-containing functional groups decreased when 4-CP was added to the aqueous iron sulfide suspensions, which likely supported the surface coverage with 4-CP. No IR bands that distinguished the FT-IR spectrum of B-FeS/4-CP from that of M-FeS/4-CP were

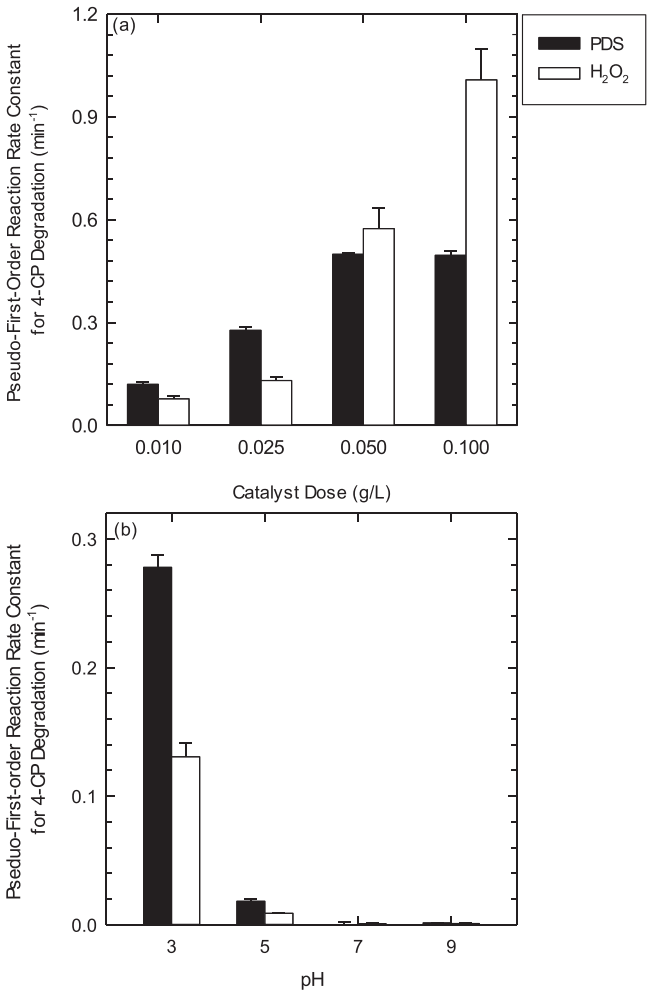

Fig. 5. Effects of (a) catalyst loading ([peroxide]$_0$ = 1 mM; [4-CP]$_0$ = 0.01 mM (for PDS) or 0.1 mM (for H_2O_2); pH_i = 3) and (b) pH on the rate of 4-CP degradation by B-FeS in the presence of H_2O_2 and PDS ([B-FeS]$_0$ = 0.025 g/L; [peroxide]$_0$ = 1 mM; [4-CP]$_0$ = 0.01 mM (for PDS) or 0.1 mM (for H_2O_2)).

observed, ruling out the likelihood that the microbial activity of *Desulfovibrio desulfuricans* enabled 4-CP degradation. Further, the presence of *Desulfovibrio desulfuricans* caused no noticeable difference in the Raman spectral features. The intensities of the peaks at 295 cm^{-1} and 380 cm^{-1} that resulted from the molecular vibration of 4-CP on iron surface [43] did not distinctively increased in the Raman spectra when 4-CP was added, which implied the weak interaction of 4-CP with sulfidated irons.

4-CP degradation followed pseudo-first-order reaction kinetics while B-FeS (or M-FeS) activated H_2O_2 and PDS, which contrasts with the biphasic reaction kinetics typically observed with nZVI: instantaneous 4-CP decay followed by drastically decelerated or almost ceased progress of 4-CP degradation (Figs. S14 and S15). This seems to result from the difference in resistance to oxidative dissolution among the iron-based activators (Fig. S16). As for nZVI, which is highly susceptible to aerobic corrosion leading to Fe(II)/Fe(III) release, oxidative 4-CP degradation exhibited two distinctive kinetic regimes: rapid 4-CP decay due to peroxide activation by nZVI and released ionic iron within an extremely short timeframe and subsequent complete inhibition via surface passivation or the radical scavenging activity of dissolved Fe(II). The role of dissolved Fe(II) and Fe(III) in peroxide activation was in line with the approximately 1.5- to 2-fold increase in the efficiencies of sulfidated iron and nZVI for 4-CP degradation when H_2O_2 was used instead of PDS (Fig. 4a). This is ascribed to the more effective Fe(II)/Fe(III) cycling by H_2O_2 than PDS, which was corroborated by the observation that Fe(II) and Fe(III) caused significant 4-CP degradation in the presence of H_2O_2, whereas 4-CP decomposition was observed solely with Fe(II)/PDS (Fig. S17).

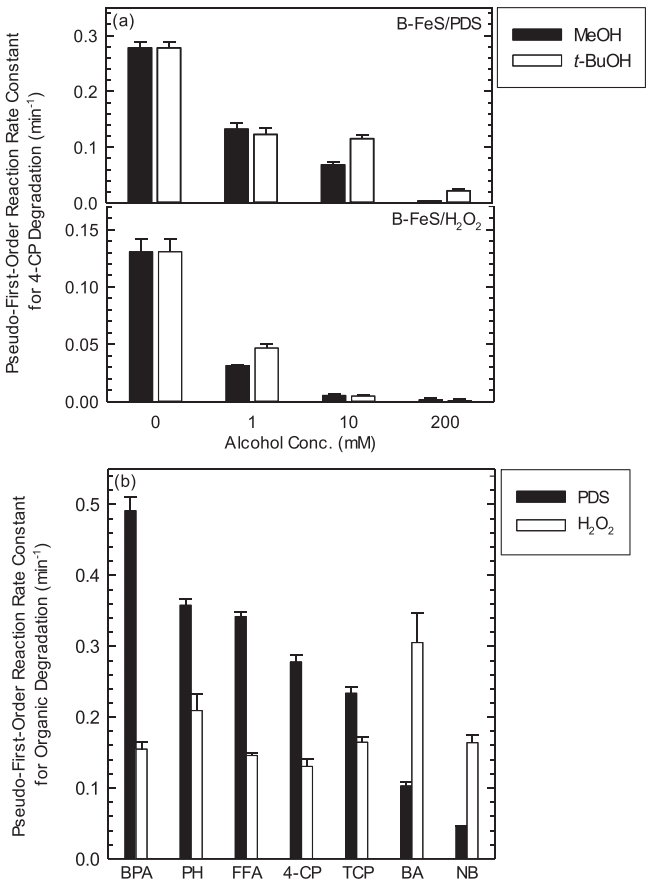

Fig. 6. (a) Effects of alcohol-based scavengers on the efficiency of B-FeS/PDS and B-FeS/H_2O_2 for 4-CP degradation ([B-FeS]$_0$ = 0.025 g/L; [peroxide]$_0$ = 1 mM; [4-CP]$_0$ = 0.01 mM (for PDS) or 0.1 mM (for H_2O_2); pH_i = 3) and (b) treatability of organic substances to oxidation by B-FeS/PDS and B-FeS/H_2O_2 ([B-FeS]$_0$ = 0.025 g/L; [peroxide]$_0$ = 1 mM; [organic compound]$_0$ = 0.01 mM (for PDS) or 0.1 mM (for H_2O_2); pH_i = 3).

3.3. *Effect of reaction parameters*

The efficiency of B-FeS for 4-CP degradation through peroxide activation was monitored as a function of catalyst loading and initial pH (Fig. 5). The experiments were designed to explore the response of the peroxide activation capability of B-FeS to the variations in the reaction parameters, rather than making a direct comparison between the two systems, namely B-FeS/PDS and B-FeS/H_2O_2. To investigate the effects of reaction parameters within a similar timeframe, PDS and H_2O_2 activation proceeded at different 4-CP concentrations; the ten-fold higher concentration of 4-CP was used for B-Fe/H_2O_2 because it was found to degrade 4-CP considerably faster than B-FeS/PDS. Regardless of the type of peroxide used, oxidative 4-CP degradation was accelerated with increasing B-FeS dosage. However, there was a moderate contrast between the two activation processes: B-FeS/H_2O_2 and B-FeS/PDS. The efficiency of B-FeS/H_2O_2 for 4-CP degradation was steadily improved without reaching a saturation point as the activator dosage was increased, whereas no further increase in the treatment efficiency was observed for B-FeS/PDS when the dosage exceeded 0.05 g/L. This is ascribed to the ability of Fe(III) to activate H_2O_2 (Fig. S17b). That is, the greater extent of treatment performance increase under the high B-FeS dosage conditions is due to the involvement of both Fe(II) and Fe(III) (oxidatively released from B-FeS) as the secondary H_2O_2 activators.

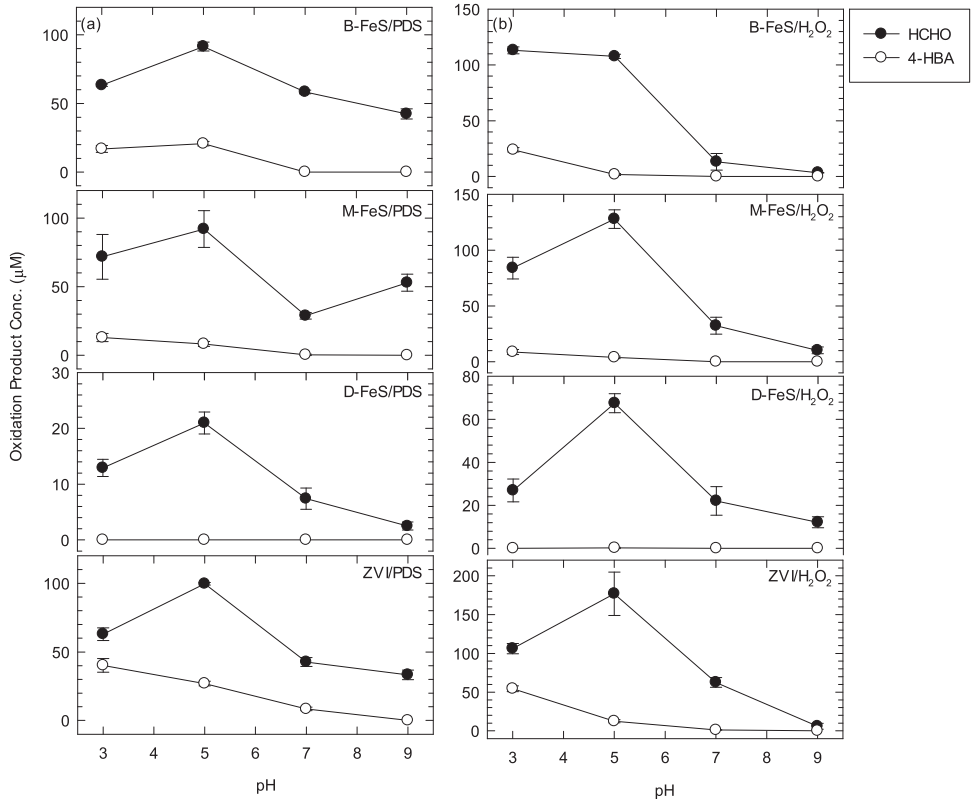

Fig. 7. Production of 4-HBA and HCHO during the oxidative degradation of BA and MeOH by the (a) PDS and (b) H_2O_2 activation systems under varying pH conditions ([iron activator]$_0$ = 0.025 g/L; [peroxide]$_0$ = 1 mM; [MeOH]$_0$ = 200 mM; [BA]$_0$ = 10 mM).

Aligned with the previous findings that acidic conditions favor peroxide activation by heterogeneous iron-based catalysts [44,45], significant 4-CP degradation occurred with B-FeS/peroxide at pH 3, and a further pH increase caused a drastic reduction in the peroxide activation capability of B-FeS, regardless of the peroxide type (Fig. 5b). Even a change in the pH from 3 to 5 decelerated oxidative 4-CP degradation by B-FeS/PDS and B-FeS/H_2O_2 by a factor of ~15, and no noticeable peroxide activation was performed under neutral and alkaline conditions, where heterogeneous iron-based activators underwent significant surface passivation and water-soluble iron species precipitated in the corresponding oxide forms.

3.4. Identification of the primary oxidants

To elucidate the main reaction pathways for organic oxidation by the biogenic iron sulfide/peroxide activation systems, B-FeS/PDS and B-FeS/H_2O_2 were examined for 4-CP degradation in the presence of MeOH and *t*-BuOH as radical scavengers (Fig. 6a). Regardless of the peroxide type, the extent to which 4-CP oxidation is kinetically retarded was more pronounced with increasing alcohol concentrations, which confirms that $SO_4^{\bullet-}$ and $^{\bullet}OH$ formed via one-electron reduction of PDS and H_2O_2, respectively, served as the main oxidants in organic oxidation. It was found that the inhibitory effects of alcohols were more significant for B-FeS/H_2O_2 because $^{\bullet}OH$ exhibits two or three orders of magnitude higher reactivity toward MeOH and *t*-BuOH than $SO_4^{\bullet-}$ [46].

The nature of the major oxidants was explored based on the treatability of seven organic substrates, namely bisphenol A (BPA), phenol (PH), furfuryl alcohol (FFA), 4-CP, 2,4,6-trichlorophenol (TCP), BA, and nitrobenzene (NB), to oxidation by PDS and H_2O_2 activated with B-FeS under acidic conditions (Fig. 6b). The efficiency of B-FeS/H_2O_2 for oxidative organic elimination exhibited the lower substrate-dependence than that of B-FeS/PDS owing to the non-selective reactivity $^{\bullet}OH$ [47] resulting from H_2O_2 activation; the pseudo-first-order reaction rate constant for B-Fe/H_2O_2 ranged from 0.15 to 0.2 min^{-1} in most cases. The relatively low substrate-specific treatment performance of B-FeS/H_2O_2 was further demonstrated based on the comparison of the two activation systems with respect to the NB treatment efficiency. It has previously been shown that NB as a substrate highly recalcitrant toward $SO_4^{\bullet-}$ is rapidly decomposed by $^{\bullet}OH$ ($k(SO_4^{\bullet-}) \leq 10^6$ $M^{-1}s^{-1}$; k ($^{\bullet}OH$) = 3.2×10^9 $M^{-1}s^{-1}$) [46]. This conformed to the observation of the effective degradation of NB by B-FeS/H_2O_2, which contrasted with the marginal progress of NB oxidation when PDS was used instead. The high susceptibility of BA to oxidative attack by $SO_4^{\bullet-}$ ($k(SO_4^{\bullet-})$ = 1.2×10^9 $M^{-1}s^{-1}$ [48]) apparently conflicts with the degradation of BA by B-FeS/PDS proceeding only two- to three-fold faster than that of NB. This reveals the involvement of high-valent iron species as secondary non-radical oxidants, considering that Fe(IV) does not readily oxidize BA [49] and causes the rapid oxidation of phenolic compounds [50]. Furthermore, the observation that MeOH significantly decelerated 4-CP degradation by B-FeS/PDS as compared to *t*-BuOH, though it reflects two or three orders of magnitude difference in the reactivity of $SO_4^{\bullet-}$ toward MeOH and *t*-BuOH, was linked to the intrinsic reactivity of high-valent iron, with k(Fe(IV) + MeOH) = 5.72×10^2 $M^{-1}s^{-1}$ and k(Fe(IV) + *t*-BuOH) = 60 $M^{-1}s^{-1}$ [51].

The efficiencies of iron-based activators such as B-FeS, M-FeS, D-FeS, and nZVI for the conversion of BA to 4-HBA and of MeOH to HCHO were monitored in the presence of PDS and H_2O_2 under varying pH conditions (Fig. 7). BA hydroxylation is typically initiated via radical addition to the benzene ring but HCHO production occurs during MeOH oxidation by high-valent iron as well as oxidizing radicals [49]. Regardless of the types of peroxide and activator, the efficiency of the conversion of BA to 4-HBA was maximized at pH 3 and the hydroxylation proceeded negligibly under non-acidic conditions. This result implies that acidic conditions favor radical generation through peroxide activation by heterogeneous iron-based catalysts. However, all tested peroxide activation systems displayed the highest HCHO formation yields at pH 5 and

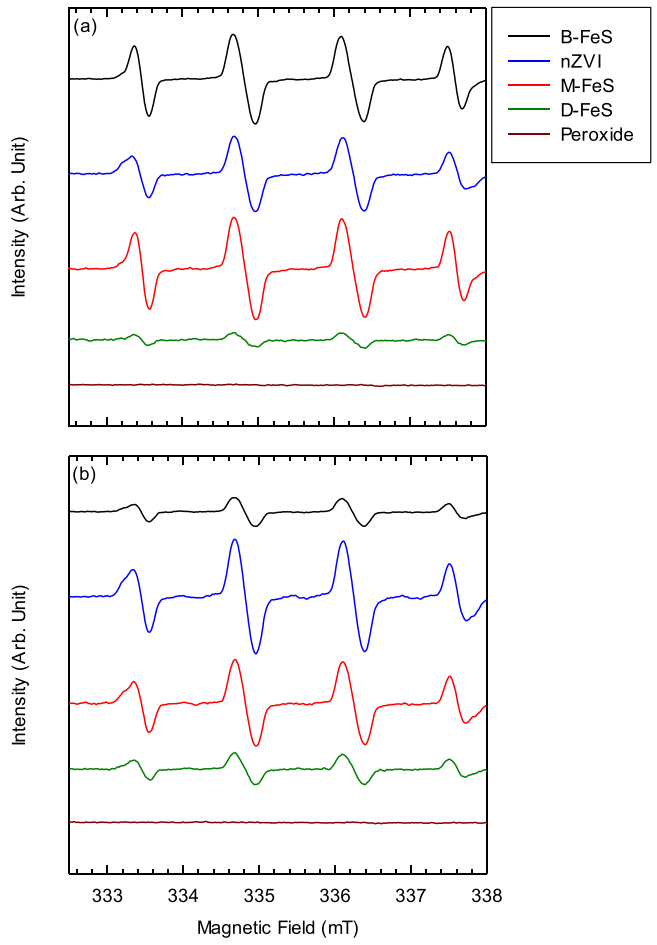

Fig. 8. EPR spectra obtained after 5-min activation of (a) PDS and (b) H_2O_2 by iron-based catalysts in the presence of BMPO as a spin trap under acidic conditions ([iron activator]$_0$ = 0.1 g/L; [peroxide]$_0$ = 1 mM; [BMPO]$_0$ = 1 mM; pH$_i$ = 3).

still enabled the significant production of HCHO from MeOH when the pH was further increased, which reveals that high-valent iron species contributed as secondary oxidants over a wide pH range. These trends, that is, BA hydroxylation and oxidative HCHO formation being optimized at pH 3 and 5, respectively, were also observed with homogenous peroxide activation by Fe(II) (Fig. S18), suggesting the involvement of dissolved Fe(II) as a peroxide activator. Notably, HCHO production was much less sensitive to pH variation when PDS was activated. For instance, the efficiency of B-FeS/PDS and M-FeS/PDS for HCHO generation was reduced by only a factor of ~2, while the pH increased from 5 to 9. In contrast, using H_2O_2 instead caused a drastic decline in HCHO production when the pH went beyond 5, almost inhibiting the conversion of MeOH to HCHO at pH 9. The results reveal that the two-electron iron oxidation leading to high-valent iron formation occurred more readily with PDS.

The EPR spectra produced during peroxide activation by iron-based materials were recorded in the presence of BMPO as a spin trap under acidic and neutral conditions (Fig. 8 and S16). In agreement with the negligible BA hydroxylation under non-acidic conditions, no noticeable EPR signals assigned to the BMPO-$^{\bullet}$OH or BMPO-$SO_4^{\bullet-}$ adducts were observed in any of the tested systems at pH 7 (Fig. S19). The distinct EPR spectra indicating $^{\bullet}$OH formation emerged while sulfidated iron and nZVI activated H_2O_2 at pH 3 (Fig. 8b), supporting the role of $^{\bullet}$OH as the major oxidant in H_2O_2 activation, as confirmed previously in Fig. 6. However, irrespective of the activator type, the EPR spectral features corresponding to the BMPO-$^{\bullet}$OH adducts dominantly appeared even when PDS was used and the signals for the BMPO-$SO_4^{\bullet-}$ adducts were insignificant (Fig. 8a). This might be due to the single electron oxidation of water/OH^- by $SO_4^{\bullet-}$ and the resultant $^{\bullet}$OH production, but the conversion of $SO_4^{\bullet-}$ to $^{\bullet}$OH is known to occur substantially at basic pH (> 10) [40]. Furthermore, the likelihood of $^{\bullet}$OH acting as the primary oxidant during PDS activation under acidic conditions conflicted with the evidence of the involvement of $SO_4^{\bullet-}$ in organic oxidation by activated PDS: substrate-dependent performance of B-FeS/PDS that conformed to the reactivity of $SO_4^{\bullet-}$ (Fig. 6b). This apparent discrepancy among the results is likely associated with the reaction between BMPO and high-valent iron as the secondary oxidant. High-valent metal species were found to oxidatively transform a nitrone spin trap (e.g., DMPO) into the corresponding aminoxyl radical via electron abstraction, yielding an EPR spectrum almost identical to that assigned to the $^{\bullet}$OH adduct [8].

3.5. Involvement of high-valent iron species

Peroxide as the two-electron oxidant is likely to produce high-valent iron from Fe(II) surface-attached to or released from sulfidated irons, although the roles of $^{\bullet}$OH and $SO_4^{\bullet-}$ as the dominating reactive species have often been demonstrated in advanced oxidation processes utilizing sulfidated irons [19,22,45]. To further explore the contribution of high-valent iron species as non-radical oxidants, the efficiencies of iron-based activators for the selective transformation of sulfoxide to sulfone via oxygen transfer unique to Fe(IV)=O^{2+} [8,52] were monitored in the presence of PDS and H_2O_2 under varying pH conditions (Fig. 9). All tested systems produced $PMSO_2$ from PMSO to varying extents, which implies the formation of Fe(IV) via iron oxidation by PDS and H_2O_2 as two-electron oxidants. In general, the PMSO-to-$PMSO_2$ conversion was more effective when PDS was used as a peroxide, as confirmed by the comparison between the PDS and H_2O_2 activation systems with respect to the ratio of $PMSO_2$ formed to PMSO consumed ($\eta[PMSO_2]$). For instance, $\eta[PMSO_2]$(PDS) at pH 3 (where the conversion was optimized) was ~89%, 77%, and 82% for B-FeS, M-FeS, and nZVI, respectively, whereas $\eta[PMSO_2](H_2O_2)$ at pH 3 was ~73%, 32%, and 27% for B-FeS, M-FeS, and nZVI, respectively. Furthermore, $\eta[PMSO_2]$ for the PDS activation systems was kept constant with increasing pH, which contrasts with $\eta[PMSO_2]$ for the H_2O_2 activation systems that sharply decreased once the pH exceeded 5. These results matched well with the dependence of the efficiency of the conversion of MeOH to HCHO (used as an indirect indication of high-valent iron formation) on the pH and peroxide type (Fig. 7). The preferential generation of high-valent iron species in the presence of PDS was also observed when two homogeneous peroxide activation systems using Fe(II) were compared in terms of $PMSO_2$ formation yield as a function of pH (Fig. S20). The role of high-valent iron species as the secondary oxidant being more critical with PDS, observed in both heterogeneous and homogeneous activation processes, is attributable to the higher oxidizing power of PDS than that of H_2O_2 (E^0(PDS) = +2.01 V_{NHE} [53]; $E^0(H_2O_2)$ = +1.78 V_{NHE} [54]).

3.6. The role of dissolved iron oxidatively released from heterogeneous iron activators

Sulfidation kinetically promotes the transfer of electrons from heterogeneous iron catalysts to PDS and H_2O_2, improving the production of peroxide-derived oxidants, namely $^{\bullet}$OH and $SO_4^{\bullet-}$ [55,56]. Further, reduced sulfur phases (i.e., S(-I), S(-II), and S(0)) in sulfidated iron are involved in the regeneration of Fe(II) from Fe(III) oxidatively dissolved from heterogeneous iron activators [19,22]. Their roles as electron sources were indirectly confirmed based on the comparison of Fe2p and S2p XPS spectra of fresh B-FeS and used B-FeS (obtained after 60-min exposure to peroxides) samples. This showed that S^{2-} as the dominant sulfur species of B-FeS almost completely vanished and oxidatively converted into S^0 and S_n^{2-} during peroxide activation, while Fe(II)

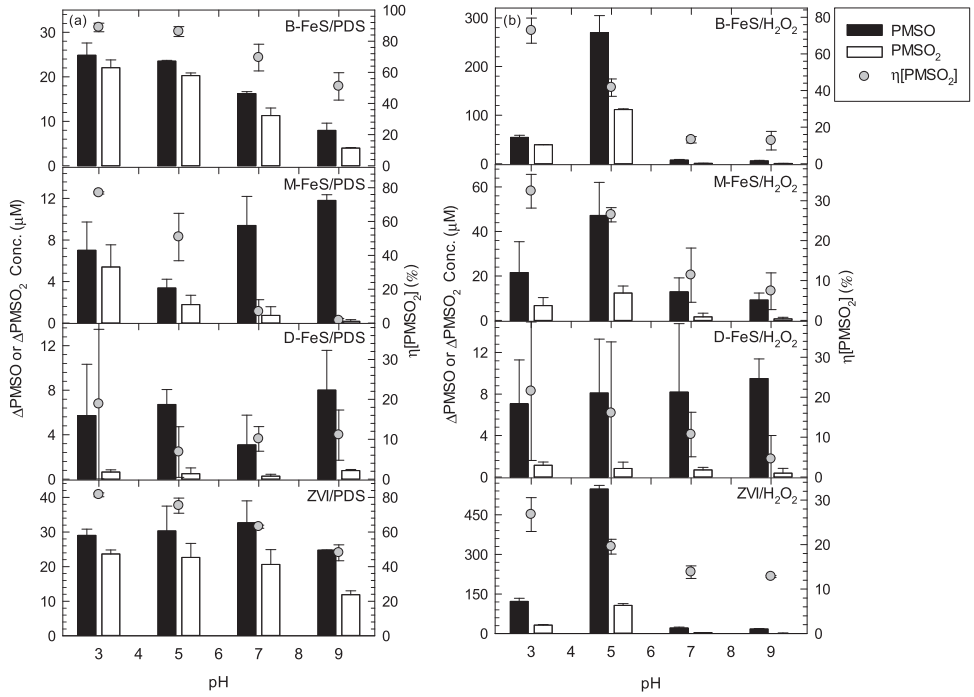

Fig. 9. Efficiency of iron-based catalysts for the conversion of PMSO to $PMSO_2$ in the presence of (a) PDS and (b) H_2O_2 under varying pH conditions ($[iron\ activator]_0$ = 0.025 g/L; $[peroxide]_0$ = 1 mM; $[PMSO]_0$ = 1 mM).

underwent partial oxidation (Fig. S21). To comparatively assess the capability of iron-based activators to facilitate Fe(II)/Fe(III) cycling, Fe (II) evolution was monitored in the aqueous suspensions of B-FeS, M-FeS, D-FeS, and nZVI upon the addition of Fe(III) (Fig. 10a). The rate of Fe(III)-to-Fe(II) conversion increased in the following order: D-FeS < M-FeS ≤ B-FeS << nZVI. The result aligns with the higher reducing power of elemental iron than that of sulfides, as confirmed by their reduction potentials ($E^0(Fe^{2+}/Fe^0) = -0.44\ V_{NHE}$ [57]; $E^0(S^0/HS^-) = -0.065\ V_{NHE}$ and $E^0(SO_4^{2-}/S^{2-}) = +0.149\ V_{NHE}$ [58]). Along with the substantial Fe(II)/Fe(III) release from nZVI (Fig. S16), facile Fe(II) regeneration by nZVI (its efficiency was approximately three-fold higher than that of B-FeS and M-FeS) would promote the reaction pathways for homogeneous peroxide activation.

The relative reducing power of the iron-based activators was indirectly compared by spectrophotometrically monitoring the time-dependent changes in absorption at 730 nm, while phosphomolybdate (PMo_{12}^{3-}) was exposed to nZVI and sulfidated iron (Fig. 10b). Since dark blue color develops as electrons are transferred to and accumulated in PMo_{12}^{3-} [59], the extent of the absorption increase quantitatively correlates to the relative reducing capacity of the heterogeneous iron activator. In agreement with the efficiency of Fe(II) regeneration (Fig. 10a), the reducing power was ranked in the following order: D-FeS < M-FeS < B-FeS << nZVI. The superiority of the electron-donating potential of B-FeS over abiotic sulfidated iron is ascribed to the higher contents of reduced sulfur species (i.e., S^{2-}) (Fig. 3), which is in line with the higher efficiency of peroxide activation (Fig. 4). The highly enhanced Fe(II) regeneration over nZVI favors radical-induced oxidation over high-valent iron-induced oxidation based on the comparison of nZVI and B-FeS with respect to $\eta[PMSO_2]$ (Fig. 7): $\eta[PMSO_2]$(PDS) at pH 3 = 82% and 91% for nZVI and B-FeS and $\eta[PMSO_2](H_2O_2)$ at pH 3 = 29% and 78% for nZVI and B-FeS. When peroxide activation was conducted on the nZVI surface, Fe(III) was effectively recovered to Fe(II) rather than being further oxidized to Fe(IV). Furthermore, the presence of Fe(II) at relatively high concentrations hinders the formation of Fe (VI) due to the comproportionation reaction: Fe(II) + Fe(VI) → 2Fe(III) [8].

The likelihood that slow Fe(II) release or regeneration could suit the high-valent iron production was explored through the comparison of HCHO and $PMSO_2$ formation yields in two Fe(II) injection modes, that is, single and split injection (Fig. 10c). As for both PDS and H_2O_2 activation systems, operation on split injection mode enhanced HCHO and $PMSO_2$ production. Notably, approximately 47% and 26% increases in HCHO and $PMSO_2$ generation, respectively, were observed when the main single injection of 0.284 mM Fe(II) (corresponding to 0.025 g/L FeS) was divided into twenty-five smaller injections performed at a constant time interval of 12 min in PDS activation. The results suggest that the relatively low availability of Fe(II) observed when sulfidated iron and PDS were used instead of nZVI and H_2O_2, respectively, caused the preferential formation of high-valent iron species.

Temporal variations in the ratio of Fe(II) and Fe(III) and SO_4^{2-} concentration were monitored with iron-based activators, namely nZVI, B-FeS, and M-FeS, in the absence and presence of peroxides (Fig. S22). Regardless of whether 4-CP was added, Fe(II) was the major iron species during the oxidative dissolution of sulfidated irons and nZVI in water. On the other hand, the relative content of Fe(III) increased upon peroxide addition, and the progress of Fe(II)-to-Fe(III) conversion implied the involvement of released Fe(II) in peroxide activation. Reflecting the role of H_2O_2 as the reducing agent in facilitating Fe(II)/Fe (III) cycling, the ratio of Fe(II) to Fe(III) was higher when H_2O_2 was used instead of PDS. The majority of ionic iron species still took the form of Fe (II) when nZVI was applied as the peroxide activator. The relative content of Fe(II) correlated well with the reducing power of iron-based activators, with the final ratio of Fe(II) to Fe(III) = 6.7%, 19.0%, and 99.1% for M-FeS, B-FeS, and nZVI in the presence of PDS, respectively. Further, the result was linked with the observation that high-valent iron species more readily formed when sulfidated irons and PDS were adopted for organic oxidation (Fig. 9); the relatively high concentrations of Fe(III) kinetically favored further oxidation of ionic irons into high-valent iron whereas effective Fe(II) regeneration facilitated the reductive conversion of peroxides into oxidizing radicals. As for all tested sulfidated irons, the release of SO_4^{2-} was not substantial and the efficiency did not noticeably increase upon H_2O_2 addition (*data not shown*). This indicated that peroxide activation initiated via electron transfer from sulfidated irons primarily caused the variation in sulfur oxidation

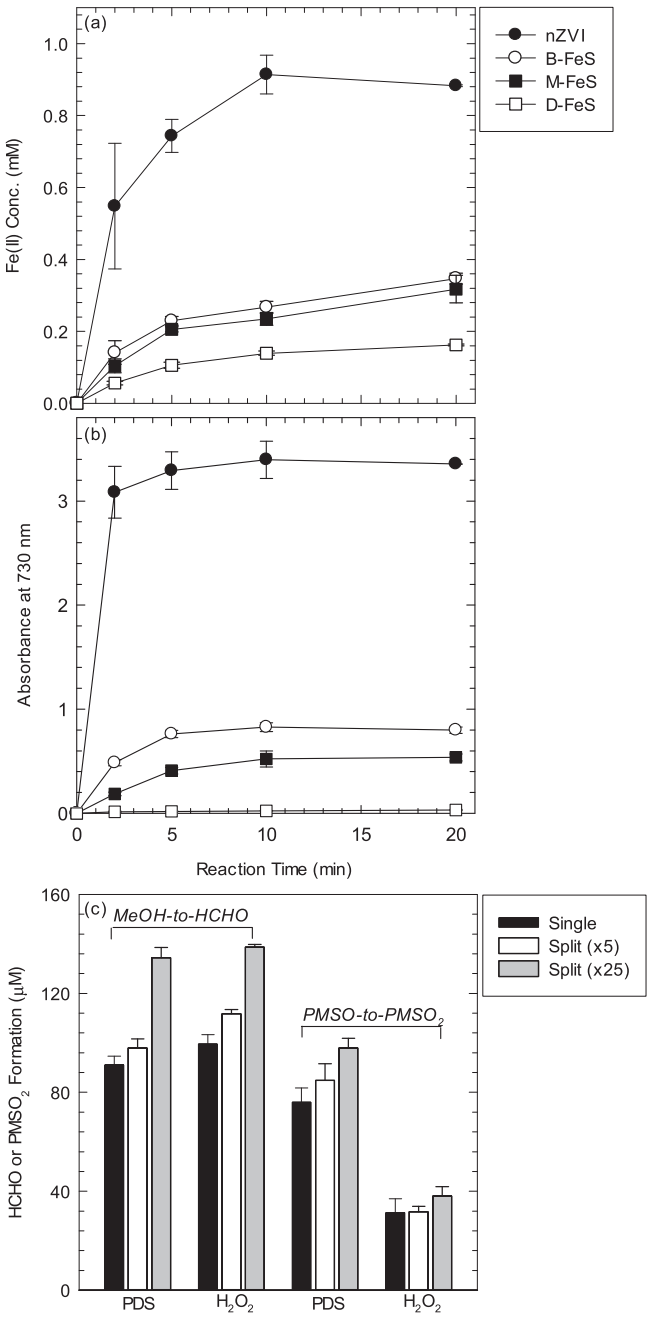

Fig. 10. (a) Fe(II) evolution upon addition of Fe(III) to the aqueous suspensions of iron-based activators ($[nZVI]_0$ = 0.1 g/L; $[sulfidated\ iron]_0$ = 0.2 g/L; $[Fe(III)]_0$ = 0.1 mM; pH_i = 3), (b) reduction of PMo_{12}^{3-} into PMo_{12}^{4-} by iron-based activators ($[nZVI]_0$ = 0.1 g/L; $[sulfidated\ iron]_0$ = 0.2 g/L; $[PMo_{12}^{3-}]_0$ = 1 mM; pH_i = 2.5), and (c) HCHO and $PMSO_2$ production in the presence of peroxides upon single and split addition of Fe(II) ($[Fe(II)]_0$ = 0.284 mM; $[peroxide]_0$ = 1 mM; $[MeOH]_0$ = 200 mM; $[PMSO]_0$ = 100 mM; pH_i = 3).

state rather than oxidative sulfur dissolution in the form of SO_4^{2-}.

3.7. Catalytic application for peroxide activation and microbially mediated regeneration

To examine catalytic peroxide activation by B-FeS, we repeatedly activated PDS and H_2O_2 using B-FeS in the same batch and explored the extent of kinetic retardation in oxidative 4-CP elimination over the six runs (Fig. 11a and b). Multiple peroxide activation was performed by

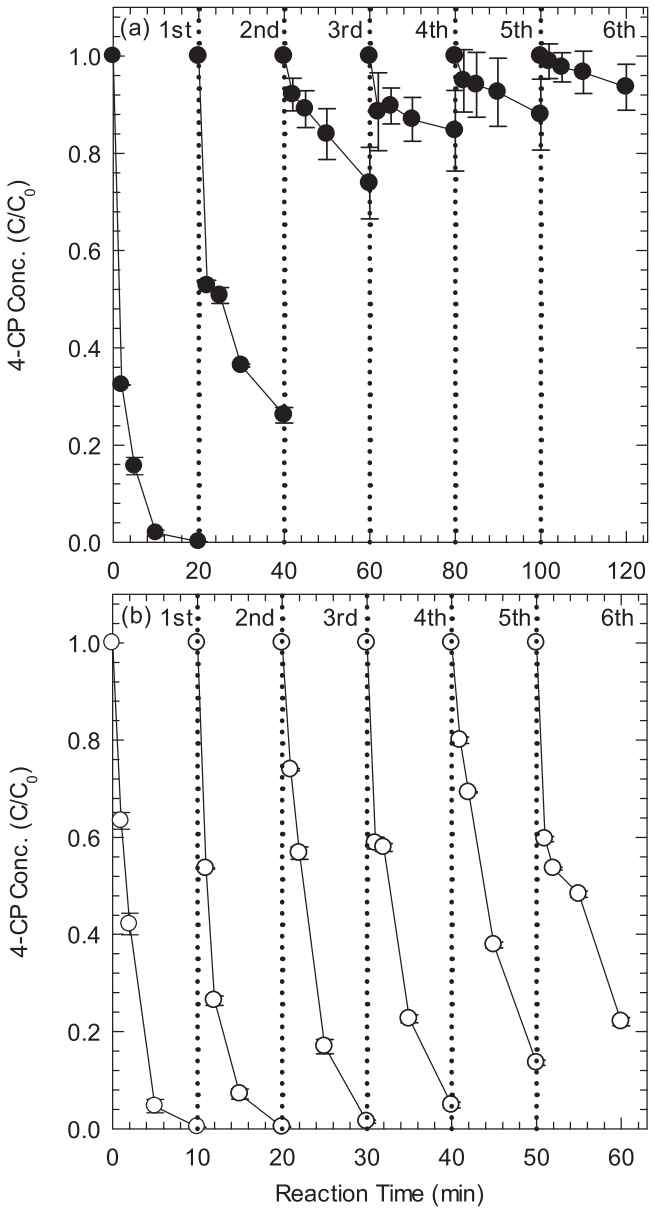

Fig. 11. Repeated 4-CP degradation by (a) B-FeS/PDS and (b) B-FeS/H_2O_2 ($[B\text{-}FeS]_0$ = 0.1 g/L; $[peroxide]_0$ = 1 mM; $[4\text{-}CP]_0$ = 0.01 mM (for PDS) or 0.1 mM (for H_2O_2); pH_i = 3).

periodically adding 4-CP and peroxide (i.e., PDS and H_2O_2) without exchanging the experimental solutions and applying fresh iron-based activators. Both PDS and H_2O_2 activation systems steadily lost the oxidizing capacity with increasing catalytic cycles, but the extent of reduction in treatment performance was much more significant with PDS. The efficiency of B-FeS/PDS for 4-CP degradation decreased by approximately 74% and 88% after the second and fourth cycles, respectively, whereas B-FeS/H_2O_2 exhibited almost constant treatment efficiency until the fourth run and underwent only a 22% reduction in the performance after the fifth cycle. The gradual loss of the peroxide activating capacity of B-FeS was the result of a combination of the decrease in the reduced iron/sulfur content, oxidative iron dissolution, and surface passivation. On top of the alteration in the chemical composition of B-FeS, intermediate accumulation that led to the undesired consumption of oxidizing radicals also caused the steady kinetic retardation in 4-CP degradation during repeated peroxide activation [60]. The relatively moderate reduction in the treatment efficiency of B-FeS/H_2O_2 was likely due to homogenous H_2O_2 activation by the

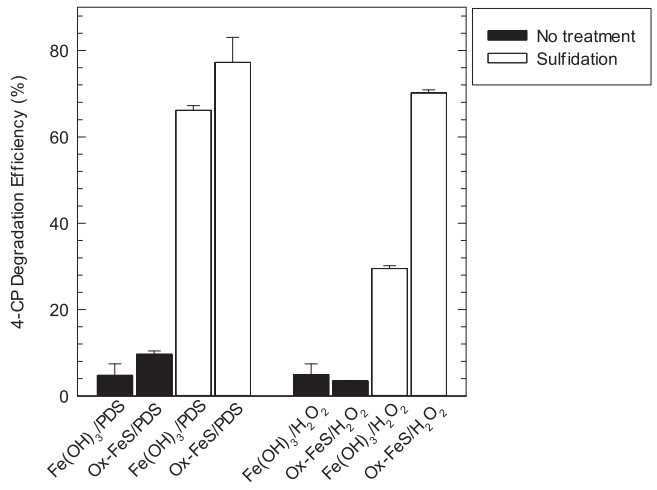

Fig. 12. 4-CP degradation during peroxide activation by microbially sulfidated amorphous $Fe(OH)_3$ and surface-oxidized B-FeS (Ox-FeS; obtained after exposure to air) ([iron-based activator]$_0$ = 0.025 g/L; [peroxide]$_0$ = 1 mM; [4-CP]$_0$ = 0.01 mM (for PDS) or 0.1 mM (for H_2O_2); pH_i = 3).

released Fe(III). Since the reductive conversion of Fe(III) to Fe(II) occurs with H_2O_2, but barely proceeds with PDS, Fe(III) selectively enabled H_2O_2 activation (Fig. S17b). The treatment efficiency was maintained over repeated cycles, particularly when H_2O_2 was used, and was also observed when nZVI was applied as an alternative peroxide activator (Fig. S23).

The possibility of biologically reactivating B-FeS that completely lost peroxide activation capability after exposure to air (hereafter referred to as Ox-FeS) was explored (Fig. 12). The reactivation of spent iron-based catalysts is highly feasible considering that surface passivation layers comprising iron oxides and hydroxides form during use of heterogeneous iron derivatives in catalytic peroxide activation [19] and the sulfidation of iron-based minerals such as ferrihydrite, goethite, and hematite is microbially achievable [61]. The progress of the surface oxidation of B-FeS was confirmed with an approximately two-fold increase in atomic oxygen content (from 27.8% to 65.7%), whereas the morphological features (i.e., agglomerates of spherical particles) were retained (Fig. S24). It was found that the XRD patterns corresponding to mackinawite crystal structures partially vanished and Fe(II) and S^{2-} transformed substantially into Fe(III) and S_n^{2-}/SO_4^{2-} (Fig. S25). Following the procedure for biotic iron sulfidation (described in Section 2.2), the anaerobic respiration of *Desulfovibrio desulfuricans* was performed in the presence of unreactive heterogeneous iron species, that is, Ox-FeS and amorphous $Fe(OH)_3$ (presumed to constitute the passivation layer that prevents interfacial electron transfer over the heterogeneous iron-based activators) (note that the dissolved Fe(II) was used for fresh B-FeS preparation). The efficiency of $Fe(OH)_3$ for 4-CP degradation in the presence of peroxides was markedly improved after $Fe(OH)_3$ was subjected to microbially mediated sulfidation, which is linked to the ability of SRB to utilize iron oxide minerals for microbial respiration [61]. The activity of Ox-FeS for PDS and H_2O_2 activation was successfully recovered to the activity level of fresh B-FeS, which implies the potential of biogenic sulfidation as a viable catalyst regeneration strategy.

4. Conclusions

This study is the first to demonstrate the potential application of microbially synthesized sulfidated iron for peroxide activation and the associated oxidative treatment of organic compounds. B-FeS achieved a higher capability for PDS and H_2O_2 activation than abiotically prepared iron-based materials, namely M-FeS, D-FeS, and nZVI based on the overall efficiency of 4-CP degradation. Notably, B-FeS outperformed the benchmark iron-based activators with respect to peroxide utilization efficiency indicating peroxide consumption required to reach a certain level of treatment efficiency. This partially resulted from the stronger resistance of B-FeS to oxidative iron dissolution that led to surface passivation and unwanted radical consumption by the released Fe(II). The relative peroxide activation performance of iron derivatives correlated with the difference in BET surface area to a certain extent. But more importantly, B-FeS was demonstrated to gain the higher reducing power than M-FeS and D-FeS due to its higher contents of reduced sulfur species based on the comparison among sulfidated irons in terms of the efficacies of Fe(III)-to-Fe(II) conversion and PMo_{12}^{3-} reduction. These are collectively linked with the superior activity of B-FeS for organic degradation via peroxide activation. Radical-induced oxidation was confirmed to be the primary degradative route during peroxide activation based on multifold evidence, which included (i) drastic deceleration in 4-CP degradation upon addition of excess alcohols, (ii) the relative susceptibility of various organics to oxidation by activated peroxides that aligned well with the reactivity of $SO_4^{\bullet-}$ and $^{\bullet}OH$, and (iii) the EPR spectral features. Alternatively, sulfidated iron/PDS exhibited relatively high efficiencies of MeOH-to-HCHO and PMSO-to-$PMSO_2$ conversion that were maintained over a broad pH range as compared to other iron/peroxide systems. The results reveal the more pronounced roles of high-valent iron species as non-radical oxidants when iron sulfide or PDS was used. This is due to the (i) high oxidizing capacity of PDS (linked to its low activity for the regeneration of Fe(II) from Fe(III)), (ii) moderate reducing power of sulfidated iron, and (iii) slow progress of oxidative Fe(II) release that resulted from the inhibited iron corrosion over sulfidated iron. Substantial sulfur oxidation that accompanied peroxide activation, confirmed by the XPS spectra of B-FeS after exposure to peroxides, implies the involvement of reduced sulfur species in Fe(II) regeneration. This is in line with the gradual reduction in treatment performance during the repeated use of B-FeS in peroxide activation. The peroxide activation capability of surface-oxidized B-FeS was confirmed to be substantially recovered once it was used as the heterogeneous electron acceptor for the anaerobic digestion of SRB, which suggests that peroxide activator regeneration was microbially achievable.

CRediT authorship contribution statement

Bowen Yang: Investigation, Validation, Writing – original draft. **Sae-In Suh**: Investigation, Validation, Methodology. **Jeonggil Lee**: Methodology. **Hwa-Soo Ryoo**: Methodology. **So-Young Ham**: Methodology. **Jaesung Kim**: Methodology. **Young-Jin Ko**: Methodology. **Heesoo Woo**: Methodology. **Jaemin Choi**: Methodology. **Hyung-Suk Oh**: Methodology. **Sang-Hoon Lee**: Methodology. **Hee-Deung Park**: Methodology, Validation. **Man Jae Kwon**: Methodology, Validation. **Hongshin Lee**: Conceptualization, Investigation, Methodology. **Jaesang Lee**: Conceptualization, Formal analysis, Writing – original draft and Revised manuscript.

Declaration of Competing Interest

The authors declare that they have no known competing financial interests or personal relationships that could have appeared to influence the work reported in this paper.

Acknowledgment

This study was supported by a National Research Foundation of Korea grant funded by the Korean government [grant no. NRF-2021R1A2C2003763], and by the Korea Ministry of Environment [grant no. RE202101610].

Appendix A. Supporting information

Supplementary data associated with this article can be found in the online version at doi:10.1016/j.apcatb.2021.120884.

References

[1] P.V. Nidheesh, Heterogeneous Fenton catalysts for the abatement of organic pollutants from aqueous solution: a review, RSC Adv. 5 (2015) 40552–40577, https://doi.org/10.1039/C5RA02023A.

[2] S. Xiao, M. Cheng, H. Zhong, Z.F. Liu, Y. Liu, X. Yang, Q.H. Liang, Iron-mediated activation of persulfate and peroxymonosulfate in both homogeneous and heterogeneous ways: a review, Chem. Eng. J. 384 (2020), 123265, https://doi.org/10.1016/j.cej.2019.123265.

[3] J. Farrell, M. Kason, N. Melitas, T. Li, Investigation of the long-term performance of zero-valent iron for reductive dechlorination of trichloroethylene, Environ. Sci. Technol. 34 (2000) 514–521, https://doi.org/10.1021/es990716y.

[4] S.H. Joo, A.J. Feitz, D.L. Sedlak, T.D. Waite, Quantification of the oxidizing capacity of nanoparticulate zero-valent iron, Environ. Sci. Technol. 39 (2005) 1263–1268, https://doi.org/10.1021/es048983d.

[5] A.L.T. Pham, F.M. Doyle, D.L. Sedlak, Kinetics and efficiency of H_2O_2 activation by iron-containing minerals and aquifer materials, Water Res. 46 (2012) 6454–6462, https://doi.org/10.1016/j.watres.2012.09.020.

[6] Z. Wang, W. Qiu, S.Y. Pang, Y. Gao, Y. Zhou, Y. Cao, J. Jiang, Relative contribution of ferryl ion species (Fe(IV)) and sulfate radical formed in nanoscale zero valent iron activated peroxydisulfate and peroxymonosulfate processes, Water Res. 172 (2020), 115504, https://doi.org/10.1016/j.watres.2020.115504.

[7] H. Lee, H.J. Lee, D.L. Sedlak, C. Lee, pH-Dependent reactivity of oxidants formed by iron and copper-catalyzed decomposition of hydrogen peroxide, Chemosphere 92 (2013) 652–658, https://doi.org/10.1016/j.chemosphere.2013.01.073.

[8] Z. Wang, J. Jiang, S.Y. Pang, Y. Zhou, C.T. Guan, Y. Gao, J. Li, Y. Yang, W. Qu, C. C. Jiang, Is sulfate radical really generated from peroxydisulfate activated by iron (II) for environmental decontamination? Environ. Sci. Technol. 52 (2018) 11276–11284, https://doi.org/10.1021/acs.est.8b02266.

[9] R.A. Crane, T.B. Scott, Nanoscale zero-valent iron: future prospects for an emerging water treatment technology, J. Hazard. Mater. 211 (2012) 112–125, https://doi.org/10.1016/j.jhazmat.2011.11.073.

[10] H.L. Lien, W.X. Zhang, Nanoscale Pd/Fe bimetallic particles: catalytic effects of palladium on hydrodechlorination, Appl. Catal. B Environ. 77 (2007) 110–116, https://doi.org/10.1016/j.apcatb.2007.07.014.

[11] D.S. Alessi, Z.H. Li, Synergistic effect of cationic surfactants on perchloroethylene degradation by zero-valent iron, Environ. Sci. Technol. 35 (2001) 3713–3717, https://doi.org/10.1021/es010564i.

[12] K.M. Sirk, N.B. Saleh, T. Phenrat, H.J. Kim, B. Dufour, J. Ok, P.L. Golas, K. Matyjaszewski, G.V. Lowry, R.D. Tilton, Effect of adsorbed polyelectrolytes on nanoscale zero valent iron particle attachment to soil surface models, Environ. Sci. Technol. 43 (2009) 3803–3808, https://doi.org/10.1021/es803589t.

[13] H.J. Zhu, Y.F. Jia, X. Wu, H. Wang, Removal of arsenic from water by supported nano zero-valent iron on activated carbon, J. Hazard. Mater. 172 (2009) 1591–1596, https://doi.org/10.1016/j.jhazmat.2009.08.031.

[14] D.M. Fan, Y. Lan, P.G. Tratnyek, R.L. Johnson, J. Filip, D.M. O'Carroll, A.N. Garcia, A. Agrawal, Sulfidation of iron-based materials: a review of processes and implications for water treatment and remediation, Environ. Sci. Technol. 51 (2017) 13070–13085, https://doi.org/10.1021/acs.est.7b04177.

[15] J.X. Li, X.Y. Zhang, Y.K. Sun, L.P. Liang, B.C. Pan, W.M. Zhang, X.H. Guan, Advances in sulfidation of zerovalent iron for water decontamination, Environ. Sci. Technol. 51 (2017) 13533–13544, https://doi.org/10.1021/acs.est.7b02695.

[16] M. Mangayayam, K. Dideriksen, M. Ceccato, D.J. Tobler, The structure of sulfidized zero-valent iron by one-pot synthesis: impact on contaminant selectivity and long-term performance, Environ. Sci. Technol. 53 (2019) 4389–4396, https://doi.org/10.1021/acs.est.8b06480.

[17] M.C. Mangayayam, J.P.H. Perez, K. Dideriksen, H.M. Freeman, N. Bovet, L. G. Benning, D.J. Tobler, Structural transformation of sulfidized zerovalent iron and its impact on long-term reactivity, Environ. Sci. Nano 6 (2019) 3422–3430, https://doi.org/10.1039/C9EN00876D.

[18] D. Cheng, A. Neumann, S.H. Yuan, W.J. Liao, A. Qian, Oxidative degradation of organic contaminants by FeS in the presence of O_2, Environ. Sci. Technol. 54 (2020) 4091–4101, https://doi.org/10.1021/acs.est.9b07012.

[19] W.Q. Guo, Q. Zhao, J.S. Du, H.Z. Wang, X.F. Li, N.Q. Ren, Enhanced removal of sulfadiazine by sulfidated ZVI activated persulfate process: performance, mechanisms and degradation pathways, Chem. Eng. J. 388 (2020), 124303, https://doi.org/10.1016/j.cej.2020.124303.

[20] Z.G. Yu, H. Rabiee, J.H. Guo, Synergistic effect of sulfidated nano zerovalent iron and persulfate on inactivating antibiotic resistant bacteria and antibiotic resistance genes, Water Res. 198 (2021), 117141, https://doi.org/10.1016/j.watres.2021.117141.

[21] Y.M. Su, D. Jassby, S.K. Song, X.F. Zhou, H.Y. Zhao, J. Filip, E. Petala, Y.L. Zhang, Enhanced oxidative and adsorptive removal of diclofenac in heterogeneous Fenton-like reaction with sulfide modified nanoscale zerovalent iron, Environ. Sci. Technol. 52 (2018) 6466–6475, https://doi.org/10.1021/acs.est.8b00231.

[22] J.H. Fan, L. Gu, D.L. Wu, Z.G. Liu, Mackinawite (FeS) activation of persulfate for the degradation of p-chloroaniline: surface reaction mechanism and sulfur-mediated cycling of iron species, Chem. Eng. J. 333 (2018) 657–664, https://doi.org/10.1016/j.cej.2017.09.175.

[23] Y. Zhou, X.L. Wang, C.Y. Zhu, D.D. Dionysiou, G.C. Zhao, G.D. Fang, D.M. Zhou, New insight into the mechanism of peroxymonosulfate activation by sulfur-containing minerals: role of sulfur conversion in sulfate radical generation, Water Res. 142 (2018) 208–216, https://doi.org/10.1016/j.watres.2018.06.002.

[24] H.R. Dong, B. Wang, L. Li, Y.Y. Wang, Q. Ning, R. Tian, R. Li, J. Chen, Q.Q. Xie, Activation of persulfate and hydrogen peroxide by using sulfide-modified nanoscale zero-valent iron for oxidative degradation of sulfamethazine: a comparative study, Sep. Purif. Technol. 218 (2019) 113–119, https://doi.org/10.1016/j.seppur.2019.02.052.

[25] C. Zhou, Y. Zhou, B.E. Rittmann, Reductive precipitation of sulfate and soluble Fe (III) by *Desulfovibrio vulgaris*: electron donor regulates intracellular electron flow and nano-FeS crystallization, Water Res. 119 (2017) 91–101, https://doi.org/10.1016/j.watres.2017.04.044.

[26] A. Picard, A. Gartman, D.R. Clarke, P.R. Girguis, Sulfate-reducing bacteria influence the nucleation and growth of mackinawite and greigite, Geochim. Cosmochim. Acta 220 (2018) 367–384, https://doi.org/10.1016/j.gca.2017.10.006.

[27] J.S. Berg, A. Duverger, L. Cordier, C. Laberty-Robert, F. Guyot, J. Miot, Rapid pyritization in the presence of a sulfur/sulfate-reducing bacterial consortium, Sci. Rep. 10 (2020), 8264, https://doi.org/10.1038/s41598-020-64990-6.

[28] Y. Yang, T.H. Chen, M. Sumona, B. Sen Gupta, Y.B. Sun, Z.H. Hu, X.M. Zhan, Utilization of iron sulfides for wastewater treatment: a critical review, Rev. Environ. Sci. Biotechnol. 16 (2017) 289–308, https://doi.org/10.1007/s11157-017-9432-3.

[29] C. Zhou, R. Vannela, K.F. Hayes, B.E. Rittmann, Effect of growth conditions on microbial activity and iron-sulfide production by *Desulfovibrio vulgaris*, J. Hazard. Mater. 272 (2014) 28–35, https://doi.org/10.1016/j.jhazmat.2014.02.046.

[30] H. Lee, H.Y. Yoo, J. Choi, I.H. Nam, S. Lee, S. Lee, J.H. Kim, C. Lee, J. Lee, Oxidizing capacity of periodate activated with iron-based bimetallic nanoparticles, Environ. Sci. Technol. 48 (2014) 8086–8093, https://doi.org/10.1021/es5002902.

[31] C.F. Wells, Spectra of 2 4-dinitrophenylhydrazone anions and determination of carbonyl compounds in dilute aqueous solution, Tetrahedron 22 (1966) 2685–2693, https://doi.org/10.1016/S0040-4020(01)99061-1.

[32] C. Liang, C.-F. Huang, N. Mohanty, R.M. Kurakalva, A rapid spectrophotometric determination of persulfate anion in ISCO, Chemosphere 73 (2008) 1540–1543, https://doi.org/10.1016/j.chemosphere.2008.08.043.

[33] A.E. Harvey, J.A. Smart, E.S. Amis, Simultaneous spectrophotometric determination of iron(II) and total iron with 1,10-phenanthroline, 1854-1854, Anal. Chem. 26 (1954), https://doi.org/10.1021/ac60097a009.

[34] C.N. Satterfield, A.H. Bonnell, Interferences in the titanium sulfate method for hydrogen peroxide, Anal. Chem. 27 (1955) 1174–1175, https://doi.org/10.1021/ac60103a042.

[35] X. Luo, W.L. Han, H. Ren, Q.Z. Zhuang, Metallic organic framework-derived Fe, N, S co-doped carbon as a robust catalyst for the oxygen reduction reaction in microbial fuel cells, Energies 12 (2019) 3846, https://doi.org/10.3390/en12203846.

[36] H. Du, C.Z. Yang, W.H. Pu, L.Y. Zeng, J.Y. Gong, Enhanced electrochemical reduction of N_2 to ammonia over pyrite FeS_2 with excellent selectivity, ACS Sustain. Chem. Eng. 8 (2020) 10572–10580, https://doi.org/10.1021/acssuschemeng.0c03675.

[37] H. Chen, Z.L. Zhang, Z.L. Yang, Q. Yang, B. Li, Z.Y. Bai, Heterogeneous Fenton-like catalytic degradation of 2,4-dichlorophenoxyacetic acid in water with FeS, Chem. Eng. J. 273 (2015) 481–489, https://doi.org/10.1016/j.cej.2015.03.079.

[38] J. Xu, A. Avellan, H. Li, X.T. Liu, V. Noel, Z.M. Lou, Y. Wang, R. Kaegi, G. Henkelman, G.V. Lowry, Sulfur loading and speciation control the hydrophobicity, electron transfer, reactivity, and selectivity of sulfidized nanoscale zerovalent iron, Adv. Mater. 32 (2020), 1906910, https://doi.org/10.1002/adma.201906910.

[39] P. Singh, P. Pal, P. Mondal, G. Saravanan, P. Nagababu, S. Majumdar, N. Labhsetwar, S. Bhowmick, Kinetics and mechanism of arsenic removal using sulfide-modified nanoscale zerovalent iron, Chem. Eng. J. 412 (2021), 128667, https://doi.org/10.1016/j.cej.2021.128667.

[40] J. Lee, U. von Gunten, J.H. Kim, Persulfate-based advanced oxidation: critical assessment of opportunities and roadblocks, Environ. Sci. Technol. 54 (2020) 3064–3081, https://doi.org/10.1021/acs.est.9b07082.

[41] J. Bandara, J.A. Mielczarski, J. Kiwi, I. Adsorption mechanism of chlorophenols on iron oxides, titanium oxide and aluminum oxide as detected by infrared spectroscopy, Appl. Catal. B Environ. 34 (2001) 307–320, https://doi.org/10.1016/S0926-3373(01)00224-7.

[42] S.L. Alderman, B. Dellinger, FTIR investigation of 2-chlorophenol chemisorption on a silica surface from 200 to 500°C, J. Phys. Chem. A 109 (2005) 7725–7731, https://doi.org/10.1021/jp051071t.

[43] R. Cheng, G.Q. Li, C. Cheng, L. Shi, X. Zheng, Z. Ma, Catalytic oxidation of 4-chlorophenol with magnetic Fe_3O_4 nanoparticles: mechanisms and particle transformation, RSC Adv. 5 (2015) 66927–66933, https://doi.org/10.1039/C5RA10433E.

[44] J.A. Bergendahl, T.P. Thies, Fenton's oxidation of MTBE with zero-valent iron, Water Res. 38 (2004) 327–334, https://doi.org/10.1016/j.watres.2003.10.003.

[45] H. Chen, Z.L. Zhang, F.B. Mingbao, W. Liu, W.J. Wang, Q. Yang, Y.N. Hu, Degradation of 2,4-dichlorophenoxyacetic acid in water by persulfate activated with FeS (mackinawite), Chem. Eng. J. 313 (2017) 498–507, https://doi.org/10.1016/j.cej.2016.12.075.

[46] C.J. Liang, H.W. Su, Identification of sulfate and hydroxyl radicals in thermally activated persulfate, Ind. Eng. Chem. Res. 48 (2009) 5558–5562, https://doi.org/10.1021/ie9002848.

[47] G.V. Buxton, C.L. Greenstock, W.P. Helman, A.B. Ross, Critical review of rate constants for reactions of hydrated electrons, hydrogen atoms and hydroxyl radicals ($^{\bullet}OH/^{\bullet}O^{-}$) in aqueous solution, J. Phys. Chem. Ref. Data 17 (1988) 513–886, https://doi.org/10.1063/1.555805.
[48] P. Neta, V. Madhavan, H. Zemel, R.W. Fessenden, Rate constants and mechanism of reaction of $SO_4^{\bullet-}$ with aromatic compounds, J. Am. Chem. Soc. 99 (1977) 163–164, https://doi.org/10.1021/ja00443a030.
[49] C.R. Keenan, D.L. Sedlak, Factors affecting the yield of oxidants from the reaction of manoparticulate zero-valent iron and oxygen, Environ. Sci. Technol. 42 (2008) 1262–1267, https://doi.org/10.1021/es7025664.
[50] H.C. Li, C. Shan, B.C. Pan, Fe(III)-doped g-C_3N_4 mediated peroxymonosulfate activation for selective degradation of phenolic compounds via high-valent iron-oxo species, Environ. Sci. Technol. 52 (2018) 2197–2205, https://doi.org/10.1021/acs.est.7b05563.
[51] O. Pestovsky, A. Bakac, Reactivity of aqueous Fe(IV) in hydride and hydrogen atom transfer reactions, J. Am. Chem. Soc. 126 (2004) 13757–13764, https://doi.org/10.1021/ja0457112.
[52] O. Pestovsky, A. Bakac, Aqueous ferryl(IV) ion: kinetics of oxygen atom transfer to substrates and oxo exchange with solvent water, Inorg. Chem. 45 (2006) 814–820, https://doi.org/10.1021/ic051868z.
[53] D.A. House, Kinetics and mechanism of oxidations by peroxydisulfate, Chem. Rev. 62 (1962) 185–203, https://doi.org/10.1021/cr60217a001.
[54] C.J. Lin, S.O. Pehkonen, The chemistry of atmospheric mercury: a review, Atmos. Environ. 33 (1999) 2067–2079, https://doi.org/10.1016/S1352-2310(98)00387-2.
[55] H. Zheng, J.G. Bao, Y. Huang, L.J. Xiang, B.X. Faheem, J.K. Ren, M.N. Du, D. D. Nadagouda, Dionysiou, Efficient degradation of atrazine with porous sulfurized Fe_2O_3 as catalyst for peroxymonosulfate activation, Appl. Catal. B Environ. 259 (2019), 118056, https://doi.org/10.1016/j.apcatb.2019.118056.
[56] J.K. Du, J.G. Bao, X.Y. Fu, C.H. Lu, S.H. Kim, Mesoporous sulfur-modified iron oxide as an effective Fenton-like catalyst for degradation of bisphenol A, Appl. Catal. B Environ. 184 (2016) 132–141, https://doi.org/10.1016/j.apcatb.2015.11.015.
[57] A.J. Bard, R. Parsons, J. Jordan, Standard Potentials in Aqueous Solution, Marcel Dekker, Inc., New York, Basel, 1985.
[58] V. Beschkov, E. Razkazova-Velkova, M. Martinov, S. Stefanov, Electricity production from marine water by sulfide-driven fuel cell, Appl. Sci. 8 (2018) 1926, https://doi.org/10.3390/app8101926.
[59] J. Lee, J. Kim, W. Choi, Oxidation on zerovalent iron promoted by polyoxometalate as an electron shuttle, Environ. Sci. Technol. 41 (2007) 3335–3340, https://doi.org/10.1021/es062430g.
[60] J. Gao, D.Q. Han, Y. Xu, Y.Y. Liu, J.G. Shang, Persulfate activation by sulfide-modified nanoscale iron supported by biochar (S-nZVI/BC) for degradation of ciprofloxacin, Sep. Purif. Technol. 235 (2020), 116202, https://doi.org/10.1016/j.seppur.2019.116202.
[61] Y.L. Li, H. Vali, J. Yang, T.J. Phelps, C.L. Zhang, Reduction of iron oxides enhanced by a sulfate-reducing bacterium and biogenic H_2S, Geomicrobiol. J. 23 (2006) 103–117, https://doi.org/10.1080/01490450500533965.